




# Adaptive Fourier Single-Pixel Imaging Based on Probability Estimation

Wei Lun Tey<sup>1</sup>, Mau-Luen Tham<sup>1</sup> <sup>a</sup>, Yeong-Nan Phua<sup>1</sup> <sup>b</sup> and Sing Yee Chua<sup>1,2</sup> <sup>c</sup>

<sup>1</sup>Lee Kong Chian Faculty of Engineering and Science, Universiti Tunku Abdul Rahman,  
Bandar Sungai Long, Selangor, Malaysia

<sup>2</sup>Centre for Photonics and Advanced Materials Research (CPAMR), Universiti Tunku Abdul Rahman,  
Bandar Sungai Long, Selangor, Malaysia

**Keywords:** Single-Pixel Imaging, Fourier Imaging, Compressed Sensing, Variable Density Sampling.

**Abstract:** Fourier single-pixel imaging (FSI) is able to reconstruct images by sampling the information in the Fourier domain. The conventional sampling method of FSI acquires the low frequency Fourier coefficients to obtain the image outlines but misses out on the image details in high frequency bands. The variable density sampling method improves the image quality but follows a predefined mechanism where the power of image information decreases when frequency increases. In this paper, an adaptive approach is proposed to sample the Fourier coefficients based on probability estimation. While the low frequency Fourier coefficients are fully sampled to secure the image outlines, the high frequency Fourier coefficients are sparsely sampled adaptively, and the image is reconstructed through Compressed sensing (CS) algorithm. Results show that the proposed adaptive FSI sampling method improves the image quality with sampling ratio ranging from 0.05 to 0.25, as compared to the commonly used conventional low frequency sampling and variable density sampling methods.


## 1 INTRODUCTION


Single-pixel imaging (SPI) is a paradigm that is only equipped with a spatially unresolved detector i.e. single-pixel detector, as compared to a conventional imaging system which employs a pixelated detector i.e. charge-coupled device or complementary metal oxide semiconductor (Gibson et al., 2020). SPI system enables the possibility of building a compact and fast imaging device at low cost, serving as an important alternative, especially in low light or unusual wavelength conditions. Choices for a single-pixel detector include a photon multiplier tube, a photodiode or a single-pixel of an image sensor (Qiu et al., 2020). Since the SPI technique was founded, it has been used in various applications such as terahertz imaging, 3D imaging (Sun et al., 2013), gas leaking detection (Gibson et al., 2017), underwater imaging (Wu et al., 2020), etc (Yu et al., 2016).


SPI samples a scene using only a single-pixel detector and a series of light modulation patterns. The image is then reconstructed from the measurements acquired by the detector with the help of reconstruction algorithms. In general, image quality and

computational complexity are the major concerns in SPI (Shin et al., 2021a; Woo et al., 2022). By introducing compressed sensing (CS) techniques, the number of measurements needed is greatly reduced to sub-Nyquist sampling rate. Pseudo-random patterns are commonly used in SPI while deterministic patterns have become popular more recently (Shin et al., 2021b). Hadamard single-pixel Imaging (HSI) and Fourier single-pixel Imaging (FSI) are the most well-known deterministic models-based techniques, using Hadamard and Fourier basis patterns respectively (Zhang et al., 2017; Yu et al., 2020). FSI is more advantageous in term of the image energy concentration as compared to HSI. Under low-sampling condition, FSI is more efficient and performs better than HSI (Zhang et al., 2017).

Zhang et al. introduced SPI through the means of Fourier spectrum acquisition (Zhang et al., 2015) and later presented different sampling strategies i.e. orderings of the Fourier basis patterns used. Conventionally, only the low frequency Fourier coefficients are sampled (Zhang et al., 2017). A sparse Fourier single-pixel imaging (S-FSI) sampling method was proposed by Meng et al. (Wenwen et al., 2019), where the sampling probability for a sampling point is inversely proportional to the distance from the center of the Fourier spectrum, namely the variable density sampling method. It improves the reconstructed im-

<sup>a</sup>  <https://orcid.org/0000-0003-4600-9839>

<sup>b</sup>  <https://orcid.org/0000-0002-7120-6626>

<sup>c</sup>  <https://orcid.org/0000-0001-6327-4592>

age in terms of signal-to-noise ratio (SNR) and object details compared to conventional FSI sampling (Hu et al., 2021). The downside of the existing variable density sampling method is that since the probability of sampling is predetermined by the distance of the sampling points from the center of Fourier spectrum, the sampling pattern is always fixed regardless of the nature and characteristics of the image. Clearly, this sampling mechanism might not be a suitable solution for all kinds of images.

The adaptive sampling method has been studied recently to address the aforementioned problem. In 2020, Liang et al. proposed an adaptive sampling trajectory based on a rough estimation of spectrum energy distribution. This method requires additional sampling and interpolation processes for the estimation (Liang et al., 2020). An adaptive sampling method based on Gaussian random sampling was proposed, where the density of the variable density sampling is based on the importance of Fourier coefficients according to 1D Gaussian function (Qiu et al., 2021). Another adaptive sampling method based on radial correlations has been proposed to produce decent image reconstruction without CS (He et al., 2021). In addition, dynamic ordering of sampling patterns based on an image dictionary was proposed (Yuan et al., 2021). Although this method is able to provide adaptive and dynamic ordering of sampling patterns based on the feedback of the recorded measurements, it requires a huge dataset to be trained before applying the image dictionary.

In this paper, an adaptive FSI sampling method based on the estimation of probability sampling is proposed without the need for training datasets. Fourier coefficients are fully sampled in the low frequency bands while the high frequency coefficients are sparsely sampled adaptively. The probability of sampling the next sampling point is decided based on the Fourier coefficient of the point sampled. This estimation is repeated in the sampling process until the targeted sampling ratio is met. Finally, the image is reconstructed using the CS algorithm. The result shows that the proposed adaptive FSI sampling method is able to produce better image quality overall compared to the conventional sampling and variable density sampling methods that are commonly implemented.

## 2 METHODOLOGY

In this section, the operating principle of conventional FSI and variable density sampling method is introduced to provide necessary background infor-

mation. Subsequently, the proposed adaptive sampling method is presented. In addition, the evaluation method is explained for the performance comparison.

### 2.1 Conventional FSI

FSI utilizes Fourier basis patterns to acquire the spectrum of the scene and then utilizes inverse fast Fourier transform (IFFT) to reconstruct the scene. The internal products of the targeted scene and the projected Fourier patterns are measured using a single-pixel detector, and all Fourier coefficients are processed through phase-shifts as shown in Eq. (1) (Qiu et al., 2021).

$$P_\phi(x, y; f_x, f_y) = a + b \cdot \cos(2\pi f_x x + 2\pi f_y y + \phi) \quad (1)$$

where  $x$  and  $y$  are the 2D Cartesian coordinates from the captured scene, while  $(f_x, f_y)$  denotes the spatial frequency,  $a$  represents the DC component,  $b$  is the contrast, and  $\phi$  indicates the initial phase. Eq. (2) can be utilized to determine the reflected intensity from the targeted scene.

$$I_\phi(f_x, f_y) = \iint_{\Omega} r(x, y) P_\phi(x, y; f_x, f_y) dx dy \quad (2)$$

where  $\Omega$  denotes the region of the targeted scene, while  $r$  represents the reflectivity distribution of the target object from the captured scene. As ambient lights fluctuate, the overall response of the detector is given in Eq. (3).

$$T_\phi(f_x, f_y) = T_n + k I_\phi(f_x, f_y) \quad (3)$$

where  $k$  is decided based on the size of the detector, while  $T_n$  indicates the ambient light measured.

Both the 4-step FSI and the 3-step FSI are acceptable but 3-step FSI reduces the measurement time by 25%. Therefore, despite the fact that 4-step FSI is more robust, 3-step FSI is preferred in practice. With a fixed phase of  $\Delta_\phi$  (i.e.,  $0, 2\pi/3, 4\pi/3$ ), 3-step FSI enables the acquisition of each Fourier coefficient based on every three corresponding illumination patterns (Hu et al., 2021). Each complex Fourier coefficient  $F(f_x, f_y)$  can therefore be obtained as:

$$F(f_x, f_y) = (2T_0 - T_{2\pi/3} - T_{4\pi/3}) + \sqrt{3}j(T_{2\pi/3} - T_{4\pi/3}) \quad (4)$$

The image can then be reconstructed by utilizing IFFT, as shown in Eq. (5).

$$r^* = IFFT(F + n) \quad (5)$$

where  $r^*$  is the under-sampled reconstructed image with noise  $n$ .

The conventional sampling method concentrates on the information in the low frequency bands of the Fourier space. Hence, only low frequency Fourier coefficients are acquired. Ringing artifacts and blur can occur since  $r^*$  lacks of high frequency coefficients (Hu et al., 2021; Mdrafai and Gurbuz, 2020).

## 2.2 Variable Density Sampling Method

Variable density FSI proposes a sampling probability based on the distance from the centre of the Fourier spectrum, as shown in Eq. (6) (Wenwen et al., 2019). As such, the power of image information slowly decreases from low to high frequencies.

$$\rho = \begin{cases} 1, & r \leq R \\ (1-r)^\epsilon, & r > R \end{cases} \quad (6)$$

$r$  denotes the distance of the sampling point to the spatial center of Fourier spectrum,  $R$  is the radius threshold in terms of sampling ratio, and positive coefficient  $\epsilon$  is to adjust the sampling probability (Wenwen et al., 2019).

The image reconstructed using variable density FSI tends to have more noise compared to the conventional sampling method but the conventional sampling method observes significant oscillation. By using the CS technique, the excessive noise can be suppressed with the cost of computation time and resources.

## 2.3 Proposed Adaptive Sampling Method

The proposed adaptive sampling method determines the probability density,  $\rho$  as shown in Eq. (7).

$$\rho = \begin{cases} 1, & r \leq R \\ \frac{coeff}{X}, & r > R \end{cases} \quad (7)$$

The proposed method suggests to fully sample the low frequency bands, represented by  $R$ .  $r$  denotes the distance of the sampling point to the spatial center of the Fourier spectrum. The probability of sampling the next sampling point is decided based on the Fourier coefficient of the point sampled  $coeff$  and threshold  $X$  which can be determined based on the low frequency coefficients sampled, as shown in Eq. (8). The threshold  $X$  is calculated based on the processed intensity matrix  $I$  which is unique per image.

$$X = I(:, :, 1) - I(:, :, 2) + I(:, :, 3) - I(:, :, 4) \quad (8)$$

As such, the probability density,  $\rho$  can be determined. Basically, Fourier coefficients in the low frequency bands are fully sampled meanwhile the coefficients in the high frequency bands are sparsely sampled adaptively. This estimation is repeated in the sampling process until the targeted sampling ratio is met.

## 2.4 Evaluation Method

Peak Signal to Noise Ratio (PSNR) represents the ratio between the maximum power possible of a signal

and noise corruption that affects the fidelity of the image's representation and are used to measure the quality of the reconstructed image. PSNR is defined based on Mean Square Error (MSE):

$$MSE = \frac{1}{M * N} \sum_{i=0, j=0}^{M-1, N-1} [I(i, j) - K(i, j)]^2 \quad (9)$$

PSNR is calculated as follow:

$$PSNR = 10 \log_{10} \left[ \frac{MAX_i^2}{MSE} \right] \quad (10)$$

where  $MAX_i^2$  represents the maximum possible value of the pixels in the image and  $MSE$  is the mean square error. The higher the PSNR, the better the quality of the reconstructed image.

Root Mean Square Error (RMSE) represents the differences between the reconstructed image and the captured scene. It is calculated as:

$$RMSE = \sqrt{MSE} \quad (11)$$

where lower values of RMSE indicates a better fit between two images with the value of 0 implying that ground truth and reconstructed image are identical.

Structural Similarity Index (SSIM) is a well-known perceptual metric that is commonly used to quantify image quality degradation. Unlike PSNR, SSIM indicates the image's visible structure. SSIM is calculated as:

$$SSIM(x, y) = \frac{(2\mu_x\mu_y + C_1)(2\sigma_{xy} + C_2)}{(\mu_x^2 + \mu_y^2 + C_1)(\sigma_x^2 + \sigma_y^2 + C_2)} \quad (12)$$

where  $\mu_x$  and  $\mu_y$  denote the pixel sample means of  $x$  and  $y$  respectively,  $\sigma_x^2$  and  $\sigma_y^2$  indicates the variance of both  $x$  and  $y$ . SSIM value ranges from 0 to 1, with the value of 1 implying an identical match between the ground truth and the reconstructed image.

## 3 RESULTS AND DISCUSSION

The study was performed using a computer equipped with an Intel(R) Core (TM) i7-11700F CPU, 32 GB RAM, and MATLAB 2021a. L1-Magic library was employed for the post-IFFT reconstruction with CS. All images were processed in a resolution of 256x256.

The performance of the proposed method is analyzed for different sampling ratios  $SR$  ranging from 0.05 to 0.25 and compared with three existing methods i.e. conventional sampling method based on circular path, variable density method (polynomial) and line mask sampling method (Qiu et al., 2021; Candes et al., 2006). Figure 1 illustrates the sampling pattern for the (a) conventional sampling method, (b) variable

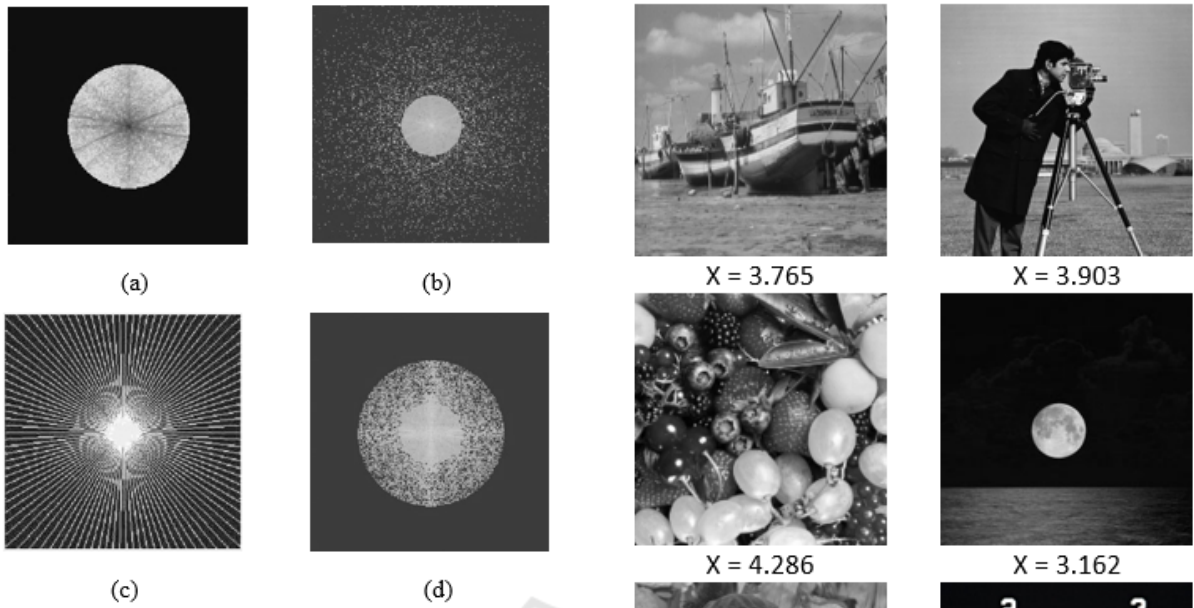


Figure 1: Sampling pattern illustration for (a) conventional sampling based on circular path, (b) variable density sampling (polynomial), (c) line mask sampling, and (d) the proposed adaptive sampling method.

density method, (c) line mask sampling method, and (d) the proposed adaptive method.

The radius threshold  $R$  is set to the same value for both the variable density sampling method and the proposed method. For  $SR = 0.05$ ,  $R$  is set to 0.03 sampling ratio while for the other  $SR > 0.05$ ,  $R$  is set to 0.05 sampling ratio. Besides, the value of  $\epsilon$  for the variable density sampling method is set as 2. With the radius  $R$  of the fully sampled low frequency bands being set to 0.05 sampling ratio, a unique threshold value,  $X$  for a particular image can be determined as shown in Figure 2.

The results comparison for two test images, ‘Pirate’ and ‘USAF chart’ are shown in Figure 3 and Figure 4. The reconstructed images using four different methods with sampling ratio  $SR$  ranging from 0.05 to 0.25 are shown respectively. The image quality is indicated by the PSNR, SSIM, and RMSE value, which serves as the quantitative comparison between the methods. It can be seen that when the sampling ratio  $SR$  increases, all four methods reconstruct images with better quality. For test image ‘Pirate’, the conventional sampling method which only samples the low frequency bands performs relatively better than the variable density sampling. This could be due to the characteristics of the test image which has more significant information in the low frequency bands. The proposed adaptive sampling method shows the best image quality among all four methods. For test



Figure 2: Threshold value,  $X$  estimated in the proposed adaptive FSI method for different test images.

image ‘USAF chart’, the variable density and the proposed adaptive sampling method outperform the conventional FSI and line mask sampling method in low sampling ratio, while line mask sampling method is comparable in high sampling ratio. This is because these methods are able to obtain high frequency details at the same time securing most image outline information in the low frequency bands.

Additional images, ‘Boat’, ‘Cameraman’, ‘Moon’ and ‘Fruits’ were tested and the results comparison using different sampling methods is summarized in Table 1. Note that the conventional sampling method outperforms the variable density sampling method on images with a more center focused spectrum such as ‘Boat’ and ‘Fruits’, while the variable density sampling method performs better on a sparser spectrum such as ‘Cameraman’ and ‘Moon’. It is worth noting that the proposed adaptive sampling approach gives the best image quality for all cases as compared to the variable density sampling method.





Sampling Ratio	Conventional FSI	Variable density FSI	Line Mask FSI	Proposed Method FSI
0.05	 PSNR = 25.281 SSIM = 0.653 RMSE = 0.054	 PSNR = 24.931 SSIM = 0.621 RMSE = 0.058	 PSNR = 20.548 SSIM = 0.462 RMSE = 0.094	 PSNR = 25.938 SSIM = 0.708 RMSE = 0.051
0.10	 PSNR = 27.385 SSIM = 0.771 RMSE = 0.043	 PSNR = 26.896 SSIM = 0.7343 RMSE = 0.045	 PSNR = 23.971 SSIM = 0.598 RMSE = 0.063	 PSNR = 28.189 SSIM = 0.801 RMSE = 0.039
0.15	 PSNR = 28.835 SSIM = 0.831 RMSE = 0.036	 PSNR = 27.875 SSIM = 0.767 RMSE = 0.040	 PSNR = 26.170 SSIM = 0.680 RMSE = 0.049	 PSNR = 29.733 SSIM = 0.854 RMSE = 0.033
0.20	 PSNR = 30.106 SSIM = 0.871 RMSE = 0.031	 PSNR = 28.767 SSIM = 0.800 RMSE = 0.036	 PSNR = 27.796 SSIM = 0.758 RMSE = 0.041	 PSNR = 30.872 SSIM = 0.889 RMSE = 0.029
0.25	 PSNR = 31.282 SSIM = 0.892 RMSE = 0.027	 PSNR = 29.749 SSIM = 0.827 RMSE = 0.033	 PSNR = 29.389 SSIM = 0.813 RMSE = 0.034	 PSNR = 31.842 SSIM = 0.913 RMSE = 0.026

Figure 3: Results comparison of different sampling methods for test image ‘Pirate’. Note that the conventional sampling method which focuses on sampling the low frequency Fourier coefficients performs relatively better than the variable density sampling. The proposed adaptive sampling method shows the best image quality among all four methods.

Sampling Ratio	Conventional FSI	Variable density FSI	Line mask FSI	Proposed Method FSI
0.05	 PSNR = 16.473 SSIM = 0.538 RMSE = 0.150	 PSNR = 17.204 SSIM = 0.723 RMSE = 0.142	 PSNR = 11.847 SSIM = 0.224 RMSE = 0.256	 PSNR = 18.040 SSIM = 0.852 RMSE = 0.125
0.10	 PSNR = 19.186 SSIM = 0.728 RMSE = 0.110	 PSNR = 21.102 SSIM = 0.896 RMSE = 0.088	 PSNR = 19.306 SSIM = 0.708 RMSE = 0.108	 PSNR = 22.925 SSIM = 0.968 RMSE = 0.071
0.15	 PSNR = 20.903 SSIM = 0.803 RMSE = 0.090	 PSNR = 25.566 SSIM = 0.935 RMSE = 0.053	 PSNR = 22.889 SSIM = 0.807 RMSE = 0.072	 PSNR = 26.122 SSIM = 0.979 RMSE = 0.049
0.20	 PSNR = 22.542 SSIM = 0.851 RMSE = 0.075	 PSNR = 30.151 SSIM = 0.961 RMSE = 0.031	 PSNR = 29.125 SSIM = 0.948 RMSE = 0.035	 PSNR = 28.839 SSIM = 0.988 RMSE = 0.026
0.25	 PSNR = 23.893 SSIM = 0.880 RMSE = 0.064	 PSNR = 33.252 SSIM = 0.973 RMSE = 0.022	 PSNR = 34.011 SSIM = 0.975 RMSE = 0.020	 PSNR = 31.967 SSIM = 0.996 RMSE = 0.022

Figure 4: Results comparison of different sampling methods for test image 'USAF chart'. Note that the variable density sampling outperforms the conventional sampling method while the proposed adaptive sampling method still shows the best image quality among all four methods overall although line mask sampling method yield higher PSNR and lower RMSE when sampling ratio increases.

Table 1: Results comparison of different sampling methods for test image ‘Boat’, ‘Cameraman’, ‘Moon’ and ‘Fruits’. Note that the conventional sampling method outperforms the variable density sampling method on images with a more center-focused spectrum such as ‘Boat’ and ‘Fruits’, while the variable density sampling method performs better on a sparser spectrum such as ‘Cameraman’ and ‘Moon’. The proposed adaptive sampling method still shows the best image quality among all four methods.

Image	Sampling Ratio	Conventional FSI			Variable Density FSI			Line Mask FSI			Proposed Method FSI		
		PSNR	SSIM	RMSE	PSNR	SSIM	RMSE	PSNR	SSIM	RMSE	PSNR	SSIM	RMSE
	0.05	24.404	0.657	0.060	23.849	0.622	0.064	20.091	0.467	0.099	<b>24.561</b>	<b>0.676</b>	<b>0.059</b>
	0.10	26.169	0.750	0.049	25.746	0.709	0.052	23.412	0.590	0.068	<b>26.740</b>	<b>0.781</b>	<b>0.046</b>
	0.15	27.690	0.819	0.041	27.043	0.761	0.044	25.343	0.679	0.054	<b>28.402</b>	<b>0.839</b>	<b>0.038</b>
	0.20	28.925	0.861	0.036	27.982	0.788	0.040	27.006	0.742	0.045	<b>29.930</b>	<b>0.871</b>	<b>0.032</b>
	0.25	30.125	0.891	0.031	28.917	0.815	0.036	28.878	0.809	0.036	<b>31.146</b>	<b>0.892</b>	<b>0.028</b>
	0.05	22.856	0.667	0.072	23.363	0.717	0.068	20.685	0.589	0.092	<b>23.811</b>	<b>0.758</b>	<b>0.064</b>
	0.10	24.463	0.749	0.060	25.599	0.783	<b>0.052</b>	23.925	0.709	0.064	<b>25.703</b>	<b>0.823</b>	<b>0.052</b>
	0.15	25.721	0.800	0.052	27.245	0.804	0.044	25.882	0.760	0.051	<b>27.289</b>	<b>0.866</b>	<b>0.043</b>
	0.20	26.717	0.834	0.046	28.940	0.828	<b>0.036</b>	27.781	0.809	0.041	<b>29.782</b>	<b>0.891</b>	<b>0.036</b>
	0.25	27.661	0.859	0.041	30.122	0.853	0.031	29.917	0.854	0.032	<b>30.972</b>	<b>0.907</b>	<b>0.028</b>
	0.05	31.753	0.850	0.026	35.054	0.893	0.018	31.863	0.851	0.026	<b>35.318</b>	<b>0.899</b>	<b>0.017</b>
	0.10	33.601	0.887	0.021	36.517	0.916	0.015	35.753	0.902	0.016	<b>37.190</b>	<b>0.932</b>	<b>0.014</b>
	0.15	34.965	0.916	0.018	37.842	0.932	0.013	36.312	0.914	0.015	<b>38.611</b>	<b>0.950</b>	<b>0.012</b>
	0.20	35.991	0.930	0.016	38.991	0.946	0.011	38.359	0.939	0.012	<b>40.141</b>	<b>0.964</b>	<b>0.010</b>
	0.25	36.918	0.942	0.014	39.788	0.954	0.010	38.806	0.947	0.011	<b>41.460</b>	<b>0.972</b>	<b>0.008</b>
	0.05	21.204	0.591	0.087	20.866	0.577	0.091	16.805	0.365	0.144	<b>21.620</b>	<b>0.637</b>	<b>0.083</b>
	0.10	23.328	0.722	0.068	22.648	0.679	0.074	19.837	0.509	0.102	<b>23.955</b>	<b>0.767</b>	<b>0.063</b>
	0.15	24.973	0.806	0.056	23.658	0.719	0.066	21.988	0.625	0.080	<b>25.832</b>	<b>0.838</b>	<b>0.051</b>
	0.20	26.311	0.853	0.048	24.715	0.762	0.058	23.679	0.704	0.065	<b>27.404</b>	<b>0.873</b>	<b>0.043</b>
	0.25	27.590	0.885	0.042	25.899	0.801	0.051	25.572	0.787	0.053	<b>28.628</b>	<b>0.896</b>	<b>0.037</b>

## 4 CONCLUSIONS

This paper proposes an adaptive approach to sample an image in the Fourier domain, which is proven to reconstruct high quality images with sub-Nyquist sampling rate. The proposed method suggests to fully sample the low frequency Fourier coefficients to secure the image outlines and adaptively sample the high frequency coefficients in a sparse manner based on the estimation of probability sampling. Accordingly, the image is reconstructed using the CS algorithm. Based on the results obtained, the proposed adaptive sampling method gives better image quality with sampling ratio ranging from 0.05 to 0.25 as compared to the existing methods i.e. conventional sampling strategy based on circular path, variable density strategy (polynomial) and line mask sampling. With the adaptive characteristic of the proposed sampling approach, it is able to perform well for various images while both the conventional sampling and variable density sampling methods do not work well in some images with peculiar Fourier spectrum patterns.

However, there are some possible improvements to be considered for the proposed method in the future. First of all, the mechanism to decide the sampling probability for spectrum points can be enhanced

by considering other conditions such as the difference in Fourier spectrum patterns. Furthermore, the CS algorithm to reconstruct the images is computationally expensive. By optimizing the algorithms to reduce the computational time and complexity, it is hoped to improve the overall efficiency of the proposed adaptive sampling method.

## ACKNOWLEDGEMENTS

The research was supported by the Ministry of Higher Education (MoHE) through Fundamental Research Grant Scheme (FRGS/1/2021/TK0/UTAR/02/9).

## REFERENCES

- Candes, E. J., Romberg, J. K., and Tao, T. (2006). Stable signal recovery from incomplete and inaccurate measurements. *Communications on Pure and Applied Mathematics: A Journal Issued by the Courant Institute of Mathematical Sciences*, 59(8):1207–1223.
- Gibson, G. M., Johnson, S. D., and Padgett, M. J. (2020). Single-pixel imaging 12 years on: a review. *Optics express*, 28(19):28190–28208.

- Gibson, G. M., Sun, B., Edgar, M. P., Phillips, D. B., Hempler, N., Maker, G. T., Malcolm, G. P., and Padgett, M. J. (2017). Real-time imaging of methane gas leaks using a single-pixel camera. *Optics express*, 25(4):2998–3005.
- He, R., Weng, Z., Zhang, Y., Qin, C., Zhang, J., Chen, Q., and Zhang, W. (2021). Adaptive fourier single pixel imaging based on the radial correlation in the fourier domain. *Optics Express*, 29(22):36021–36037.
- Hu, Y., Cheng, Z., Fan, X., Liang, Z., and Zhai, X. (2021). Optimizing the quality of fourier single-pixel imaging via generative adversarial network. *Optik*, 227:166060.
- Liang, Z., Yu, D., Cheng, Z., and Zhai, X. (2020). Adaptive fourier single-pixel imaging sampling based on frequency coefficients prediction. *Optical Engineering*, 59(7):073105.
- Mdrafi, R. and Gurbuz, A. C. (2020). Joint learning of measurement matrix and signal reconstruction via deep learning. *IEEE Transactions on Computational Imaging*, 6:818–829.
- Qiu, Z., Guo, X., Lu, T., Qi, P., Zhang, Z., and Zhong, J. (2021). Efficient fourier single-pixel imaging with gaussian random sampling. In *Photonics*, volume 8, page 319. MDPI.
- Qiu, Z., Zhang, Z., Zhong, J., et al. (2020). Comprehensive comparison of single-pixel imaging methods. *Optics and Lasers in Engineering*, 134:106301.
- Shin, Z., Chai, T.-Y., Pua, C. H., Wang, X., and Chua, S. Y. (2021a). Efficient spatially-variant single-pixel imaging using block-based compressed sensing. *Journal of Signal Processing Systems*, 93(11):1323–1337.
- Shin, Z., Lin, H. S., Chai, T.-Y., Wang, X., and Chua, S. Y. (2021b). Programmable spatially variant single-pixel imaging based on compressive sensing. *Journal of Electronic Imaging*, 30(2):021004.
- Sun, B., Edgar, M. P., Bowman, R., Vittert, L. E., Welsh, S., Bowman, A., and Padgett, M. J. (2013). 3d computational imaging with single-pixel detectors. *Science*, 340(6134):844–847.
- Wenwen, M., Dongfeng, S., Jian, H., Kee, Y., Yingjian, W., and Chengyu, F. (2019). Sparse fourier single-pixel imaging. *Optics express*, 27(22):31490–31503.
- Woo, B. H., Tham, M.-L., and Chua, S. Y. (2022). Deep learning based single pixel imaging using coarse-to-fine sampling. In *2022 IEEE 18th International Colloquium on Signal Processing & Applications (CSPA)*, pages 127–131. IEEE.
- Wu, H., Zhao, M., Li, F., Tian, Z., and Zhao, M. (2020). Underwater polarization-based single pixel imaging. *Journal of the Society for Information Display*, 28(2):157–163.
- Yu, W.-K., Yao, X.-R., Liu, X.-F., Lan, R.-M., Wu, L.-A., Zhai, G.-J., and Zhao, Q. (2016). Compressive microscopic imaging with “positive–negative” light modulation. *Optics Communications*, 371:105–111.
- Yu, X., Yang, F., Gao, B., Ran, J., and Huang, X. (2020). Deep compressive single pixel imaging by reordering hadamard basis: a comparative study. *IEEE Access*, 8:55773–55784.
- Yuan, A. Y., Feng, J., Jiao, S., Gao, Y., Zhang, Z., Xie, Z., Du, L., and Lei, T. (2021). Adaptive and dynamic ordering of illumination patterns with an image dictionary in single-pixel imaging. *Optics Communications*, 481:126527.
- Zhang, Z., Ma, X., and Zhong, J. (2015). Single-pixel imaging by means of fourier spectrum acquisition. *Nature communications*, 6(1):1–6.
- Zhang, Z., Wang, X., Zheng, G., and Zhong, J. (2017). Hadamard single-pixel imaging versus fourier single-pixel imaging. *Optics Express*, 25(16):19619–19639.